JACS
JOURNAL OF THE AMERICAN CHEMICAL SOCIETY
pubs.acs.org/JACS

Open Access
This article is licensed under CC-BY 4.0

Communication

Large Multichannel Architectures in Three-Dimensional Covalent Organic Frameworks for Efficient Guest Diffusion

Chenxi Xiong,[§] Hui Zhou,[§] Jiaming Zhou, Artit Jarusarunchai, Nuoqian Yan, Yoonseob Kim, Kwanwoo Nam, Dong-Myeong Shin,* and Seungkyu Lee*

Cite This: J. Am. Chem. Soc. 2026, 148, 15370−15376

Read Online

ACCESS | Metrics & More | Article Recommendations | Supporting Information

ABSTRACT: Guest diffusion in bulk covalent organic frameworks (COFs) is fundamentally limited by misaligned layers in two-dimensional (2D) frameworks and discontinuous 1D channels in 2D and 3D COFs across crystallite boundaries. Here, we report new triptycene-based 3D COFs, HKU-2-PEG*n* (HKU: The University of Hong Kong; *n* = 2 or 4), featuring orthogonally interconnected channels and tunable polyethylene glycol (PEG) functionality that mitigate the diffusion limitations. These COFs contain channels up to 4.8 nm in width and a total of 67 channels larger than 5 Å (13 crystallographically unique) distributed along multiple crystallographic directions, facilitating channel connectivity between randomly oriented crystallites. Lithium-ion (Li^+) transport in bulk samples of these COFs exhibits high diffusion coefficients across a wide range of Li^+ concentrations, comparable to those of commercial liquid electrolytes, demonstrating that large, multichannel crystalline architectures effectively mitigate the diffusion anisotropy inherent to low-dimensional channels in COFs.

Covalent organic frameworks (COFs) are crystalline porous materials constructed from organic molecular units linked by strong covalent bonds.[1−3] Reticular design enables precise control over connectivity, topology, and pore functionality in COFs, which is essential for diverse guest diffusion and interaction-related applications, such as gas storage and separation and energy storage.[4−6]

Guest diffusion in COFs is strongly influenced by lattice geometry, channel size, and functional groups installed.[7−11] One-dimensional (1D) channels in 2D and 3D COFs have been widely studied for adsorption, separation, and catalysis and shown to support efficient diffusion.[12−18] However, in principle, diffusion in the 1D channels of layered COFs can be hindered by layer misalignment.[19−21] In bulk samples, diffusion through 1D channels of 2D and 3D COFs can be restricted by random crystal orientation.[22,23] In contrast, 3D interconnected large channels have the potential to provide multidirectional pathways that reduce anisotropy, shorten detours around obstacles, and promote faster diffusion across diverse guest-migration scenarios.[22]

Bulky and flexible functional groups within COF channels can substantially alter the local dielectric environment, thereby modulating guest diffusion and solvation.[24−27] Recent studies have demonstrated that incorporating such substituents—such as amine-bearing polymeric aliphatic chains for direct air capture and long polyethylene glycol chains for ion solvation—can induce selective diffusion and solvation in COFs.[28−32] Despite this promise, COFs that integrate bulky functional groups within 3D interconnected large channels remain rare.[22,33] The construction of 3D COFs with multiple large channels is inherently challenging, and the introduction of bulky, flexible linkers further complicates synthesis by disrupting lattice assembly and often yielding amorphous materials.[34−36] Achieving large-pore 3D COFs that are readily functionalized would enable systematic investigations of mass transport across a wide range of guest-migration conditions.

Here, we report a new family of 3D COFs, HKU-2-PEG*n* (HKU: The University of Hong Kong; PEG: polyethylene glycol; *n* = 2 or 4), featuring 67 total channels (13 unique channels with apertures >5 Å) homogeneously and angularly distributed throughout a crystallite. With the largest pore aperture of 4.8 × 4.2 nm^2, these channels are densely functionalized with long, flexible PEG chains, which provide desirable solvation environments for effective ion transport.[37] The frameworks are in **acs**-topology and constructed by using a trigonal-prismatic node, 2,3,6,7,14,15-hexakis(4-aminophenyl)triptycene (HAPT), to induce a 3D topology, and a linear dialdehyde linker, 2,5-bis(2-(2-methoxyethoxy)-ethoxy)terephthalaldehyde (TAPEG*n*, *n* = 2 or 4), to increase node separation and open large channel apertures.[34] The PEG chains occupy the channel volume, offering abundant interaction sites and promoting strong solvation with guest ions.

To evaluate the transport advantages of the designed architectures under realistic conditions, lithium-ion (Li^+) migration was examined in bulk samples composed of randomly oriented crystallites. The materials exhibit room-temperature ionic conductivities of 0.74−1.20 mS cm^{-1} and high Li^+ transference numbers of 0.62−0.65. The extracted Li^+ diffusion coefficient reaches 1.6 × 10^{-7} cm^2 s^{-1} at low Li^+

Received: January 21, 2026
Revised: March 18, 2026
Accepted: March 25, 2026
Published: April 13, 2026



ACS Publications
© 2026 The Authors. Published by American Chemical Society

https://doi.org/10.1021/jacs.6c01500
J. Am. Chem. Soc. 2026, 148, 15370−15376

Downloaded from pubs.acs.org/jacsat/article-pdf/148/15/15370/6493781 1/ja6c01500.pdf by EWHA WOMANS UNIV user on 29 September 2026

concentrations, comparable to values reported for commercial liquid LiTFSI-propylene carbonate electrolytes. These experimental results indicate that the large multichannel architecture sustains intrinsic Li^+ mobility despite random crystallite orientation.

Consistent with this observation, molecular dynamics simulations show that Li^+ diffusion remains nearly isotropic even when pore overlap between neighboring crystallites is reduced to ~50%, enabled by transport through the interconnected three-dimensional channel network.

HKU-2-PEG2 and -PEG4 were synthesized via a reversible imine condensation between HAPT and TAPEG2 and TAPEG4, respectively (Figure 1 and S1 to S14). In the synthesis condition, 2,2,2-trifluoroethylamine (TFEA) was used to control the crystallization kinetics, and trifluoroacetic acid (TFA) was used as a catalyst to improve the crystallinity.[38,39] Single crystals with a trigonal morphology and an average size of ~5 μm were obtained at the bottom of the reaction vials after heating at 40 °C for 7 days. Attempts to synthesize HKU-2 using a nonfunctionalized aldehyde linker instead produced an unknown phase crystal. The structure of HKU-2 could not be determined from the available PXRD data and is currently under further investigation (Figure S15).

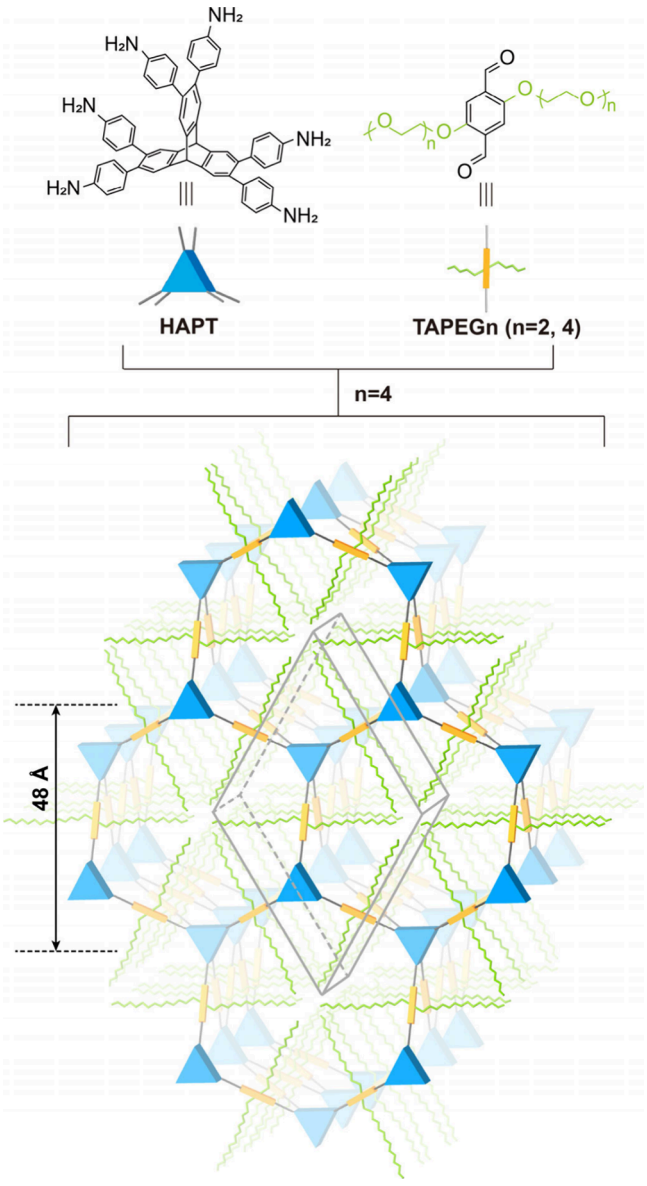


Figure 1. Structures of the building units and HKU-2-PEG*n* (*n* = 4). The blue trigonal prism represents HAPT, the linker is shown in gray, and the green chains represent the PEG units.

The structures of HKU-2-PEG2 and -PEG4 were validated by modeling their structures and comparing the simulated PXRD patterns with the experimentally obtained ones (Figure 2a and 2b). Both crystals were modeled in space group $P6_3/m$ and unit cell parameters, a = 41.60 Å and c = 22.80 Å for HKU-2-PEG2 and a = 41.93 Å and c = 26.20 Å for HKU-2-PEG4. The Pawley refinement suggested that the simulated patterns from the unit cell parameters are in good agreement with experimental patterns, with R_p and R_{wp}, values of 3.63% and 5.27% for HKU-2-PEG4 and 1.39% and 1.81% for HKU-2-PEG4. Potential 2-fold interpenetrated versions of both COFs were modeled, and their simulated PXRD patterns were studied (Figure S16−S21 and Table S1). HKU-2-PEG4 presents larger unit cell parameters compared to HKU-2-PEG2, consistent with the significantly bulkier PEG chains occupying a larger pore volume. Molecular simulations indicate that the PEG chains preferentially adopt wall-associated conformations instead of fully spanning or blocking the channel interiors. As a result, while partial pore occupation by PEG is expected and indeed contributes to the solvation environment for Li^+, continuous ion-transport pathways remain accessible. The Fourier-transform infrared (FT-IR) spectra of the COFs displayed a characteristic peak of imine (C=N) bonds at 1609 cm^{-1}, confirming the successful imine bond formation (Figure 2c and S24). Additionally, the disappearance of N−H stretching bands (3300−3500 cm^{-1}) from HAPT and a noticeable attenuation of the C=O stretching vibrations at 1678 cm^{-1} for TAPEG2 and 1683 cm^{-1} for TAPEG4 further support imine bond formation. SEM images (Figure 2d to g) revealed aggregated polyhedral particles, where HKU-2-PEG4 displayed higher uniformity than did HKU-2-PEG2. TEM images showed well-defined lattice fringes, confirming the high crystallinity of the COFs (Figure 2h and i). For HKU-2-PEG2, a lattice spacing of 36.0 Å was observed, corresponding to the (100) plane of the framework. In HKU-2-PEG4, the spacing slightly increases to 36.3 Å, indicating that the longer PEG chains induce a slight expansion.

The channel architecture of HKU-2-PEG4 was analyzed by rotating the crystal structure along multiple crystallographic axes (Figure 3 and Supporting Information Section 2.6). The orientations of these channels relative to the principal axis are illustrated in Figures 3a and 3b. Three distinct channel sets are present: one channel parallel to the principal axis, seven channels located along either the crystal edges or faces, and five channels occupying complementary positions. The channels are occupied by flexible and disordered PEG chains. Channel dimensions were measured between the arrowheads in Figure 3 without accounting for the van der Waals radii of the atoms. Eight unique channels with both width and height exceeding 10 Å were identified, providing sufficient space for the diffusion of small molecules and ions (Figure 3c to j). An additional five narrower channels (channel size between 5 and 10 Å) are shown in Figure 3k and 3o. By applying symmetry operations, including the 6_3 screw axis, inversion center, and mirror plane, to the 13 crystallographically unique channels and excluding overlapping ones, a total of 67 channels were identified within

Downloaded from pubs.acs.org/jacsat/article-pdf/148/15/15370/6493781 1/ja6c01500.pdf by EWHA WOMANS UNIV user on 29 September 2026

https://doi.org/10.1021/jacs.6c01500
J. Am. Chem. Soc. 2026, 148, 15370−15376

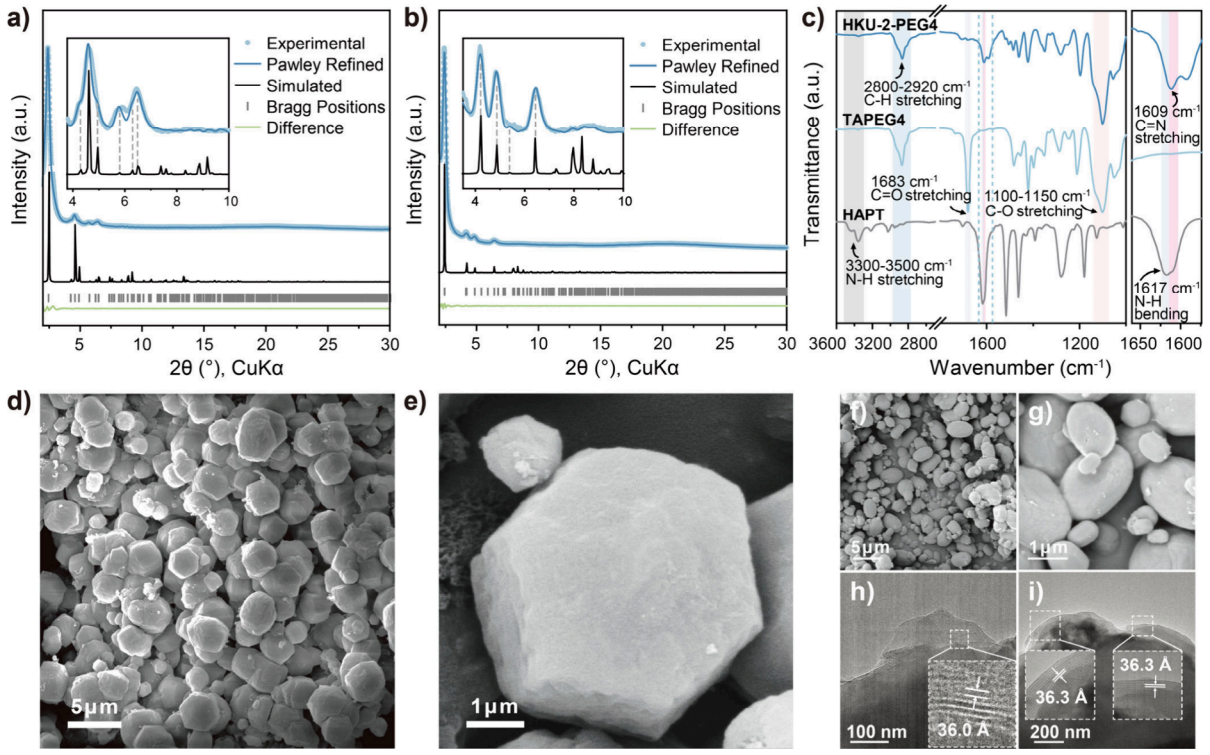


Figure 2. Structural and morphological analysis of HKU-2-PEG*n* (a) and (b) PXRD patterns of HKU-2-PEG2 and -PEG4, respectively. (c) FT-IR spectra of HKU-2-PEG2, TAPEG2, and HAPT. (d) and (e) SEM images of HKU-2-PEG4. (f) and (g) SEM images of HKU-2-PEG2. TEM images of (h) HKU-2-PEG2 and (i) HKU-2-PEG4.

a single crystal. These channels are well distributed angularly throughout the structure. Such an isotropic channel distribution increases the likelihood that when two crystallites come into contact with random orientations, even a small angular offset can bring their channels into alignment, thereby enabling intercrystallite channel connectivity.

The ionic conductivities and transference numbers (t_{Li+}) of Li^+-doped COFs soaked in propylene carbonate (PC) were examined using electrochemical impedance spectroscopy (Figure S35), which was then analyzed to determine the Li^+ diffusion coefficients (D_{Li+}) (Supporting Information Section S3.4). At room temperature (25 °C), Li^+@HKU-2-PEG2 exhibits a high conductivity of 0.74 mS cm^{-1}, while Li^+@HKU-2-PEG4 reaches 1.20 mS cm^{-1} (Figure 4a). Li^+@HKU-2-PEG2 delivered a t_{Li+} value of 0.62, while Li^+@HKU-2-PEG4 achieved a similarly high value of 0.65 (Figure S36 and S37). For diffusion analysis, we investigated Li^+ transport at varying Li^+ salt concentrations, where the Li^+ concentration is defined as the molar ratio of Li^+ incorporated in the COF framework to the total amount of PC added to the electrolyte phase (Figure 4b). At low concentrations (~2.8 M), Li^+@HKU-2-PEG4 exhibits the D_{Li+} of 9.94 × 10^{-8} cm^2 s^{-1}, which is in excellent agreement with D_{Li+} in bulk PC solution,[40] and this value decreases to 4.97 × 10^{-9} cm^2 s^{-1} at elevated concentration (25.5 M). We attribute a lower diffusion coefficient at high concentration to ion pairing, in tandem with a change in solvation structure arising from the diminished PC/Li^+ ratio.[41,42] The activation energy calculated from the Arrhenius plot is 0.26 eV (Figure 4c), which is comparable to the bulk LiTFSI-PC system.[43] To gain further insight into the mass transport in the COFs, the dominant diffusion mode of Li^+ was assessed by comparing the characteristic diffusion length of Li^+ (L_c) to the radius of its solvation shell (L_s). The characteristic length L_c can be quantified from the residence time of a solvation-shell member (τ_{res}^{PC}) and the D_{Li+} using the Einstein relation:[44]

$$L_c = \sqrt{6D_{Li+}\tau_{res}^{PC}}$$

where τ_{res}^{PC} was extracted from extrapolations (Figure S41) of the experimental data reported by Pan et al.,[45] and we set L_s = 6.6 Å in this study.[45,46] Figure 4d displays the L_c/L_s ratios obtained for each Li^+ concentration. Across all concentrations examined, L_c/L_s remains below unity, suggesting that diffusion occurred predominantly through solvation-shell reconfiguration rather than through solvation-cluster migration. This result is consistent with the experimental results[45] and the molecular dynamics (MD) simulation[44] of the liquid LiTFSI-PC system. Given low PC/Li^+ ratios compared to the favorable coordination number (~4 PC/Li^+),[47,48] the ether groups in PEG chains likely form clusters with Li^+ in the process of diffusion throughout COFs. Enhanced Li^+ mobility in Li^+@HKU-2-PEG4 (Figure 4b) corroborates enhanced ion solvation by ether groups arising from a greater number of coordination sites in longer PEG chains.

We performed MD simulations to elucidate the multidirectional Li^+ transport pathways across the COFs. As illustrated in Figure 4e, two crystallites in contact were constructed with systematically varied degrees of interlayer pore misalignment. This misalignment was precisely tuned by shifting the HAPT moieties along the principal channel axis, corresponding to the largest pore dimension (48 Å). The four dislocations studied in this work are 6, 12, 18, and 24 Å, corresponding to pore overlaps spanning 87.5 to 50.0%. Figure 4f displays the diagonal diffusion coefficients in Li^+-doped HKU-2-PEG4 as a function of differing pore overlaps. The D_{Li+} of COF with no

https://doi.org/10.1021/jacs.6c01500
J. Am. Chem. Soc. 2026, 148, 15370−15376

Downloaded from pubs.acs.org/jacsat/article-pdf/148/15/15370/6493781 1/ja6c01500.pdf by EWHA WOMANS UNIV user on 29 September 2026

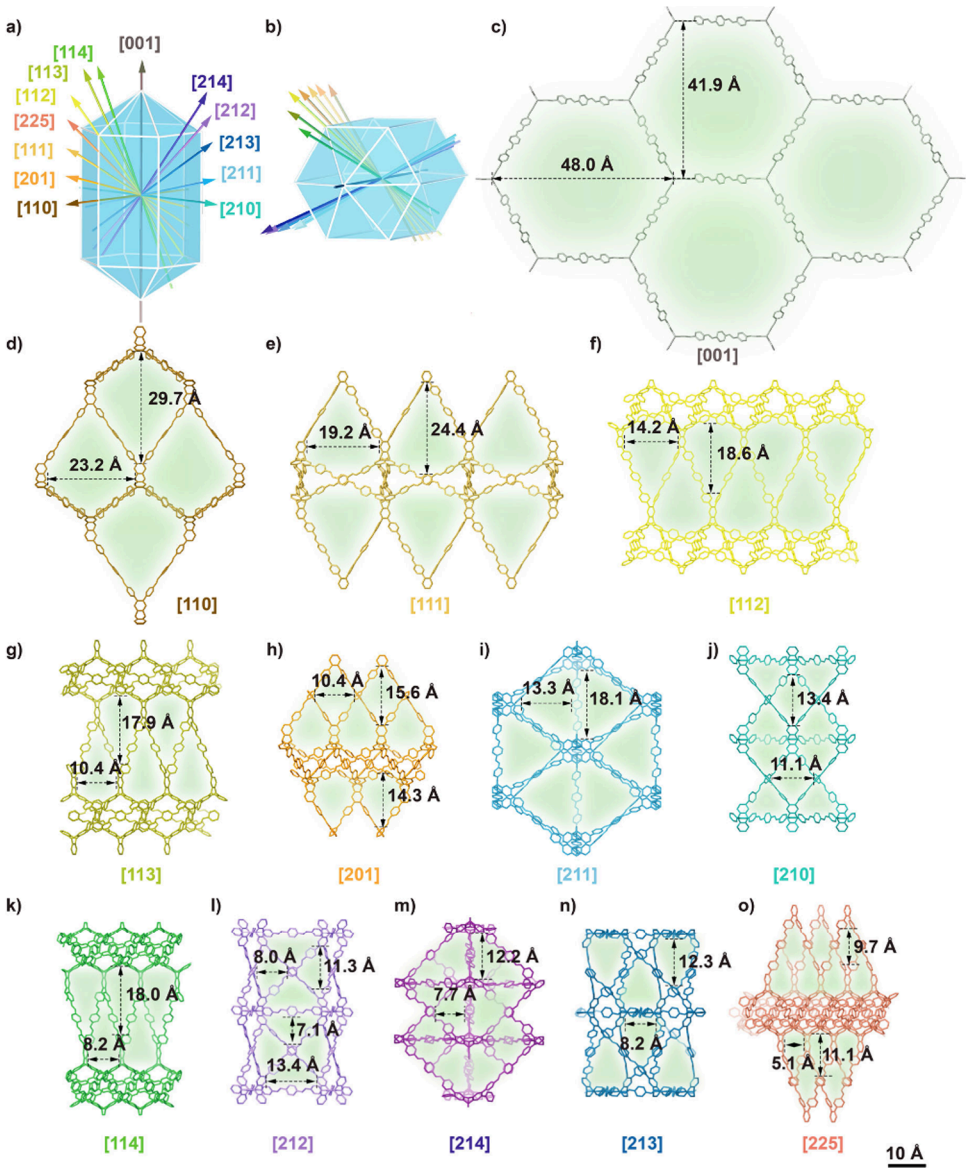


Figure 3. Channel structures and orientations in HKU-2-PEG4. (a and b) Relative orientations of the channels within a single crystal. Channel projections with both height and width greater than 10 Å (c to j) and between 5 Å and 10 Å (k to o). The frame colors correspond to the arrow colors in (a) and (b), indicating their respective directions. The labeled distances denote the separations between the arrow tips. The green pore regions represent disordered and flexible PEG chains occupying the channels.

misalignment was determined from MD simulations to be 5.82 × 10^{-8} cm^2 s^{-1}, agreeing with the experimentally measured value (4.26 × 10^{-8} cm^2 s^{-1}) at the given Li^+ concentration. It is worth noting that isotropic diffusion was observed in HKU-2-PEG4, indicating that the multiple channels reduce anisotropy in mass transport, whereas directional diffusion was found to be dominant in the 2D ionic COF (iCOF).[49] Additionally, visualizing the trajectories in Li^+@HKU-2-PEG2 (see Movie S1 and Figure S42) reveals a tortuous path where Li^+ ions interact with both immobile pore-confined PC molecules and skeletal ether groups, confirming the active role of PEG chains in coordinating Li^+.

Even after pore misalignments were introduced, it was shown that the isotropic diffusion and its coefficient remained similar, suggesting that the interconnected channels shorten the detours around obstacles. We note that the 62.5% pore overlap slightly increases the diffusion coefficient (~6%), largely due to the placement of ether moieties in close proximity, which improves ion solvation. Similar results were observed for HKU-2-PEG2 (Figure S40).

In summary, we have developed new 3D COFs, HKU-2-PEG*n* (*n* = 2 or 4), featuring well-defined, orthogonally interconnected channel networks that enable multidirectional Li^+ transport in a crystallite. Li^+ diffusion was quantitatively evaluated by diffusion coefficients derived from impedance measurements across a wide range of salt concentrations, revealing a strong dependence on the solvation structure and ion pairing. Analysis of characteristic diffusion lengths indicates that Li^+ migration proceeds predominantly through solvation-shell reconfiguration, with PEG groups participating in Li^+ coordination, particularly in frameworks bearing longer PEG chains. MD simulations further demonstrate that the interconnected 3D channel architecture supports largely isotropic Li^+ diffusion and effectively mitigates the impact of pore misalignment. This work highlights the importance of

https://doi.org/10.1021/jacs.6c01500
J. Am. Chem. Soc. 2026, 148, 15370−15376

Downloaded from pubs.acs.org/jacsat/article-pdf/148/15/15370/6493781 1/ja6c01500.pdf by EWHA WOMANS UNIV user on 29 September 2026

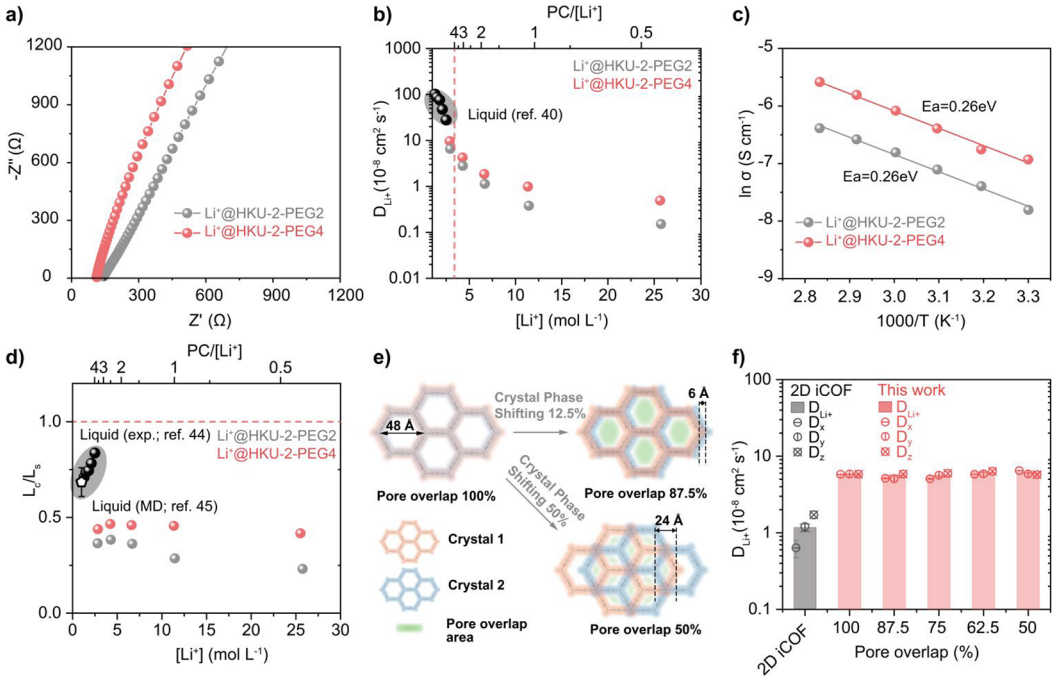


Figure 4. Diffusivity within Li$^+$@HKU-2-PEG*n* (*n* = 2 or 4). (a) Nyquist plots of EIS measurements of Li$^+$@HKU-2-PEG*n* COFs. (b) Diffusion coefficients for Li$^+$ in Li$^+$@HKU-2-PEG*n*. Black circles indicate Li$^+$ diffusion coefficients at low concentration in PC solution.[40] (c) Arrhenius plot of ionic conductivity as a function of temperature for Li$^+$@HKU-2-PEG*n* COFs. (d) Ratio of the characteristic diffusion length (L_c) to the solvation shell radius (L_s). *Black pentagon and circles are L_c/L_s from MD simulations and experimental results at low concentration, respectively.*[44,45] *(e) Schematic illustration of pore misalignment in Li$^+$@HKU-2-PEG4. (f) Diagonal diffusion coefficients for Li$^+$ in Li$^+$@HKU-2-PEG4. Gray data points are simulation results of 2D iCOF.*[49]

large multiple channels in 3D COFs in enabling efficient guest diffusion.

■ ASSOCIATED CONTENT

Supporting Information

The Supporting Information is available free of charge at https://pubs.acs.org/doi/10.1021/jacs.6c01500.

Movie S1. Visualization of the trajectories in Li$^+$@HKU-2-PEG2 (MP4)

Synthesis and characterization of the reported COFs, including TGA, FTIR, optical microscope images, and N_2 isotherm measurements (PDF)

■ AUTHOR INFORMATION

Corresponding Authors

Dong-Myeong Shin − *Department of Mechanical Engineering, The University of Hong Kong, Pokfulam, Hong Kong SAR, China;* orcid.org/0000-0002-5402-9947; Email: dmshin@hku.hk

Seungkyu Lee − *Department of Chemistry, The University of Hong Kong, Pokfulam, Hong Kong SAR, China;* orcid.org/0000-0003-3680-5882; Email: skchem@hku.hk

Authors

Chenxi Xiong − *Department of Chemistry, The University of Hong Kong, Pokfulam, Hong Kong SAR, China;* orcid.org/0009-0005-0725-6863

Hui Zhou − *Department of Mechanical Engineering, The University of Hong Kong, Pokfulam, Hong Kong SAR, China*

Jiaming Zhou − *Department of Mechanical Engineering, The University of Hong Kong, Pokfulam, Hong Kong SAR, China*

Artit Jarusarunchai − *Department of Chemistry, The University of Hong Kong, Pokfulam, Hong Kong SAR, China;* orcid.org/0009-0004-0339-1606

Nuoqian Yan − *Department of Chemistry, The University of Hong Kong, Pokfulam, Hong Kong SAR, China*

Yoonseob Kim − *Department of Chemical and Biological Engineering, The Hong Kong University of Science and Technology, Hong Kong SAR, China;* orcid.org/0000-0002-6892-8281

Kwanwoo Nam − *Department of Chemical Engineering and Materials Science, Ewha Womans University, Seoul 03760, South Korea;* orcid.org/0000-0003-0505-7228

Complete contact information is available at: https://pubs.acs.org/10.1021/jacs.6c01500

Author Contributions

§C.X. and H.Z. contributed equally.

Notes

The authors declare no competing financial interest.

■ ACKNOWLEDGMENTS

We gratefully acknowledge financial support from the Research Grants Council of Hong Kong under the Early Career Scheme (No. 27308123), Environment and Conservation Fund (No. 239/2024), and the Collaborative Research Fund (Award No. C6047-23G) of the Research Grants Council of the Hong Kong Special Administrative Region, China. We also thank the staffs at the Shanghai Synchrotron Radiation Facility (SSRF, China) for their assistance at BL17B1 and BL03HB (Project Nos. 2023-NFPS-PT-500591, 2024-NFPS-PT-500979, 2024-SSRF-HZ-505601).

https://doi.org/10.1021/jacs.6c01500
J. Am. Chem. Soc. 2026, 148, 15370−15376

Downloaded from pubs.acs.org/jacsat/article-pdf/148/15/15370/6493781/jja6c01500.pdf by EWHA WOMANS UNIV user on 29 September 2026

REFERENCES

(1) Côté, A. P.; Benin, A. I.; Ockwig, N. W.; O'Keeffe, M.; Matzger, A. J.; Yaghi, O. M. Porous, Crystalline, Covalent Organic Frameworks. *Science* **2005**, *310*, 1166−1170.

(2) El-Kaderi, H. M.; Hunt, J. R.; Mendoza-Cortés, J. L.; Côté, A. P.; Taylor, R. E.; O'Keeffe, M.; Yaghi, O. M. Designed Synthesis of 3D Covalent Organic Frameworks. *Science* **2007**, *316*, 268−272.

(3) Diercks, C. S.; Yaghi, O. M. The atom, the molecule, and the covalent organic framework. *Science* **2017**, *355*, eaal1585.

(4) Ding, S.-Y.; Wang, W. Covalent organic frameworks (COFs): from design to applications. *Chem. Soc. Rev.* **2013**, *42*, 548−568.

(5) Zhao, X.; Pachfule, P.; Thomas, A. Covalent organic frameworks (COFs) for electrochemical applications. *Chem. Soc. Rev.* **2021**, *50*, 6871−6913.

(6) Wang, Z.; Zhang, S.; Chen, Y.; Zhang, Z.; Ma, S. Covalent organic frameworks for separation applications. *Chem. Soc. Rev.* **2020**, *49*, 708−735.

(7) Yang, J.; Wang, B.; Feng, X. Mass Transport Based on Covalent Organic Frameworks. *Acc. Chem. Res.* **2025**, *58*, 1447−1460.

(8) Wang, Z.; Yang, Y.; Zhao, Z.; Zhang, P.; Zhang, Y.; Liu, J.; Ma, S.; Cheng, P.; Chen, Y.; Zhang, Z. Green synthesis of olefin-linked covalent organic frameworks for hydrogen fuel cell applications. *Nat. Commun.* **2021**, *12*, 1982.

(9) Fenton, J. L.; Burke, D. W.; Qian, D.; Olvera de la Cruz, M.; Dichtel, W. R. Polycrystalline Covalent Organic Framework Films Act as Adsorbents, Not Membranes. *J. Am. Chem. Soc.* **2021**, *143*, 1466−1473.

(10) Liu, S.; Wei, L.; Zeng, T.; Jiang, W.; Qiu, Y.; Yao, X.; Wang, Q.; Zhao, Y.; Zhang, Y.-B. Single-Crystal Dynamic Covalent Organic Frameworks for Adaptive Guest Alignments. *J. Am. Chem. Soc.* **2024**, *146*, 34053−34063.

(11) Irie, T.; Sasaki, K.; Nozaki, M.; Kawawaki, T.; Das, S.; Negishi, Y. Beyond the Multicomponent Debus-Radziszewski Route: Two-Component Cyclocondensation Constructing a 12 + 3-Connected aea Topology Three-Dimensional Imidazole-Linked COF for Sustainable Wastewater Treatment. *J. Am. Chem. Soc.* **2026**, *148*, 9527−9539.

(12) Liang, X.; Tian, Y.; Yuan, Y.; Kim, Y. Ionic Covalent Organic Frameworks for Energy Devices. *Adv. Mater.* **2021**, *33*, 2105647.

(13) Zhang, L.; Wang, S.; Zhou, Y.; Wang, C.; Zhang, X.-Z.; Deng, H. Covalent Organic Frameworks as Favorable Constructs for Photodynamic Therapy. *Angew. Chem., Int. Ed.* **2019**, *58*, 14213−14218.

(14) Natraj, A.; Ji, W.; Xin, J.; Castano, I.; Burke, D. W.; Evans, A. M.; Strauss, M. J.; Ateia, M.; Hamachi, L. S.; Gianneschi, N. C.; Alothman, Z. A.; Sun, J.; Yusuf, K.; Dichtel, W. R. Single-Crystalline Imine-Linked Two-Dimensional Covalent Organic Frameworks Separate Benzene and Cyclohexane Efficiently. *J. Am. Chem. Soc.* **2022**, *144*, 19813−19824.

(15) Xue, T.; Peng, L.; Liu, C.; Li, R.; Qiu, R.; Qian, Y.; Guan, X.; Shi, S.; Xu, G.; Zhu, L.; Yang, S.; Li, J.; Jiang, H.-L. Synthesis of high quality two dimensional covalent organic frameworks through a self-sacrificing guest strategy. *Nat. Commun.* **2025**, *16*, 2023.

(16) Su, Y.; Li, B.; Xu, H.; Lu, C.; Wang, S.; Chen, B.; Wang, Z.; Wang, W.; Otake, K.-i.; Kitagawa, S.; Huang, L.; Gu, C. Multi-Component Synthesis of a Buta-1,3-diene-Linked Covalent Organic Framework. *J. Am. Chem. Soc.* **2022**, *144*, 18218−18222.

(17) Liu, P.; Song, Z.; Huang, Q.; Xu, Z.; Lv, Y.; Gan, L.; Liu, M. Tri(Thiophene-Nitrile) Covalent Organic Frameworks With Low HOMO/LUMO Donor/Acceptor for High-Potential-Plateau Zinc Batteries. *Angew. Chem., Int. Ed.* **2026**, *65*, e25690.

(18) Almarza, J.; Strutyński, K.; Fu, S.; Chen, Y.; Padial, N. M.; del Barrio Gómez, I.; Martí-Gastaldo, C.; Khlobystov, A. N.; Bonn, M.; Wang, H. I.; Melle-Franco, M.; Mateo-Alonso, A. High Charge Carrier Mobility in Non-Conjugated 3D Covalent Organic Frameworks. *Adv. Mater.* **2026**, e17211.

(19) Cao, Y.; Wang, M.; Wang, H.; Han, C.; Pan, F.; Sun, J. Covalent Organic Framework for Rechargeable Batteries: Mechanisms and Properties of Ionic Conduction. *Adv. Energy Mater.* **2022**, *12*, 2200057.

(20) Castano, I.; Evans, A. M.; Reis, R. d.; Dravid, V. P.; Gianneschi, N. C.; Dichtel, W. R. Mapping Grains, Boundaries, and Defects in 2D Covalent Organic Framework Thin Films. *Chem. Mater.* **2021**, *33*, 1341−1352.

(21) Emmerling, S. T.; Schuldt, R.; Bette, S.; Yao, L.; Dinnebier, R. E.; Kästner, J.; Lotsch, B. V. Interlayer Interactions as Design Tool for Large-Pore COFs. *J. Am. Chem. Soc.* **2021**, *143*, 15711−15722.

(22) Chen, J.; Tang, Z.; Sheng, L.; Li, Z.; Zhu, D.; Wang, J.; Tang, Y.; He, X.; Xu, H. 3D Covalent Organic Framework Membrane with Interactive Ion Nanochannels for Hydroxide Conduction. *J. Am. Chem. Soc.* **2025**, *147*, 3714−3723.

(23) Kim, Y.; Li, C.; Huang, J.; Yuan, Y.; Tian, Y.; Zhang, W. Ionic Covalent Organic Framework Solid-State Electrolytes. *Adv. Mater.* **2024**, *36*, 2407761.

(24) Lee, W.; Li, H.; Du, Z.; Feng, D. Ion transport mechanisms in covalent organic frameworks: implications for technology. *Chem. Soc. Rev.* **2024**, *53*, 8182−8201.

(25) Guan, X.; Fang, Q.; Yan, Y.; Qiu, S. Functional Regulation and Stability Engineering of Three-Dimensional Covalent Organic Frameworks. *Acc. Chem. Res.* **2022**, *55*, 1912−1927.

(26) Huang, N.; Wang, P.; Jiang, D. Covalent organic frameworks: a materials platform for structural and functional designs. *Nat. Rev. Mater.* **2016**, *1*, 16068.

(27) Yang, Y.; Zeng, K.; Feng, Y.; An, Q.; Liu, L.; Ren, F.; Liang, X.; Zhao, G.; Zhi, S.; Guo, H. Modulating Electron Delocalization Structure in Covalent Organic Frameworks Through Conjugation and Hybridization to Boost Li-ion Migration Dynamics. *Angew. Chem., Int. Ed.* **2026**, *65*, e25864.

(28) Zhou, Z.; Ma, T.; Zhang, H.; Chheda, S.; Li, H.; Wang, K.; Ehrling, S.; Giovine, R.; Li, C.; Alawadhi, A. H.; Abduljawad, M. M.; Alawad, M. O.; Gagliardi, L.; Sauer, J.; Yaghi, O. M. Carbon dioxide capture from open air using covalent organic frameworks. *Nature* **2024**, *635*, 96−101.

(29) Zhang, G.; Hong, Y.-l.; Nishiyama, Y.; Bai, S.; Kitagawa, S.; Horike, S. Accumulation of Glassy Poly(ethylene oxide) Anchored in a Covalent Organic Framework as a Solid-State Li+ Electrolyte. *J. Am. Chem. Soc.* **2019**, *141*, 1227−1234.

(30) Xu, Q.; Tao, S.; Jiang, Q.; Jiang, D. Ion Conduction in Polyelectrolyte Covalent Organic Frameworks. *J. Am. Chem. Soc.* **2018**, *140*, 7429−7432.

(31) Guo, C.; Xue, P.; Feng, W.; Yang, Y.; Zhou, L.; Zhuang, H.; Chen, Y.; Chen, Y.; Lan, Y.-Q. Covalent Organic Framework Quantum Dots for Near-Frictionless Ion Transport Battery Electrolyte. *Angew. Chem., Int. Ed.* **2025**, *64*, No. e202512031.

(32) Wang, Y.; Zhang, K.; Jiang, X.; Liu, Z.; Bian, S.; Pan, Y.; Shan, Z.; Wu, M.; Xu, B.; Zhang, G. Branched Poly(ethylene glycol)-Functionalized Covalent Organic Frameworks as Solid Electrolytes. *ACS Appl. Energy Mater.* **2021**, *4*, 11720−11725.

(33) Zhu, T.; Kong, Y.; Lyu, B.; Cao, L.; Shi, B.; Wang, X.; Pang, X.; Fan, C.; Yang, C.; Wu, H.; Jiang, Z. 3D covalent organic framework membrane with fast and selective ion transport. *Nat. Commun.* **2023**, *14*, 5926.

(34) Li, H.; Chen, F.; Guan, X.; Li, J.; Li, C.; Tang, B.; Valtchev, V.; Yan, Y.; Qiu, S.; Fang, Q. Three-Dimensional Triptycene-Based Covalent Organic Frameworks with ceq or acs Topology. *J. Am. Chem. Soc.* **2021**, *143*, 2654−2659.

(35) Zheng, H.; Li, H.; Ji, J.; Chen, F.; Wang, Y.; Suo, J.; Song, J.; Zhao, D.; Valtchev, V.; Qiu, S.; Fang, Q. Topological Derivative Strategy for Large-Pore Three-Dimensional Covalent Organic Frameworks. *J. Am. Chem. Soc.* **2025**, *147*, 39223−39231.

(36) Wu, M.; Huang, H.; Xu, B.; Zhang, G. Poly(ethylene glycol)-functionalized 3D covalent organic frameworks as solid-state polyelectrolytes. *RSC Adv.* **2022**, *12*, 16354−16357.

(37) Fenton, D. E.; Parker, J. M.; Wright, P. V. Complexes of alkali metal ions with poly(ethylene oxide). *Polymer* **1973**, *14*, 589.

(38) Han, J.; Feng, J.; Kang, J.; Chen, J.-M.; Du, X.-Y.; Ding, S.-Y.; Liang, L.; Wang, W. Fast growth of single-crystal covalent organic frameworks for laboratory x-ray diffraction. *Science* **2024**, *383*, 1014−1019.

Downloaded from pubs.acs.org/jacsat/article-pdf/148/15/15370/6493781 1/ja6c01500.pdf by EWHA WOMANS UNIV user on 29 September 2026

https://doi.org/10.1021/jacs.6c01500
J. Am. Chem. Soc. 2026, 148, 15370−15376

(39) Ma, T.; Kapustin, E. A.; Yin, S. X.; Liang, L.; Zhou, Z.; Niu, J.; Li, L.-H.; Wang, Y.; Su, J.; Li, J.; Wang, X.; Wang, W. D.; Wang, W.; Sun, J.; Yaghi, O. M. Single-crystal x-ray diffraction structures of covalent organic frameworks. *Science* **2018**, *361*, 48−52.
(40) Karatrantos, A. V.; Ohba, T.; Cai, Q. Diffusion of ions and solvent in propylene carbonate solutions for lithium-ion battery applications. *J. Mol. Liq.* **2020**, *320*, 114351.
(41) Suo, L.; Hu, Y.-S.; Li, H.; Armand, M.; Chen, L. A new class of Solvent-in-Salt electrolyte for high-energy rechargeable metallic lithium batteries. *Nat. Commun.* **2013**, *4*, 1481.
(42) Alshangiti, O.; Galatolo, G.; Rees, G. J.; Guo, H.; Quirk, J. A.; Dawson, J. A.; Pasta, M. Solvent-in-Salt Electrolytes for Fluoride Ion Batteries. *ACS Energy Lett.* **2023**, *8*, 2668−2673.
(43) Nishida, T.; Nishikawa, K.; Fukunaka, Y. Diffusivity Measurement of LiPF6, LiTFSI, LiBF4 in PC. *ECS Trans.* **2008**, *6*, 1.
(44) Borodin, O.; Smith, G. D. LiTFSI Structure and Transport in Ethylene Carbonate from Molecular Dynamics Simulations. *J. Phys. Chem. B* **2006**, *110*, 4971−4977.
(45) Pan, J.; Charnay, A. P.; Zheng, W.; Fayer, M. D. Revealing Lithium Ion Transport Mechanisms and Solvation Structures in Carbonate Electrolytes. *J. Am. Chem. Soc.* **2024**, *146*, 35329−35338.
(46) Self, J.; Fong, K. D.; Persson, K. A. Transport in Superconcentrated LiPF6 and LiBF4/Propylene Carbonate Electrolytes. *ACS Energy Lett.* **2019**, *4*, 2843−2849.
(47) Wang, Y.; Xu, H.; Cao, B.; Ma, J.; Yu, Z. In Situ Species Analysis of a Lithium-Ion Battery Electrolyte Containing LiTFSI and Propylene Carbonate. *J. Phys. Chem. Lett.* **2024**, *15*, 5047−5055.
(48) Mynam, M.; Ravikumar, B.; Rai, B. Molecular dynamics study of propylene carbonate based concentrated electrolyte solutions for lithium ion batteries. *J. Mol. Liq.* **2019**, *278*, 97−104.
(49) Cheng, L.; Deng, Y.; Huang, J.; Zhang, Z.; Duan, H.; Kim, Y.; Wang, Y. Atomistic Transport Mechanisms in Lithium Salt-Doped Ionic Covalent Organic Framework Electrolytes. *Batteries Supercaps* **2025**, *8*, No. e202400580.

Downloaded from pubs.acs.org/jacsat/article-pdf/148/15/15370/6493781 1/ja6c01500.pdf by EWHA WOMANS UNIV user on 29 September 2026

https://doi.org/10.1021/jacs.6c01500
J. Am. Chem. Soc. 2026, 148, 15370−15376